

University of Reading
Department of Mathematics

Ageostrophic Wind Storms in the Central Caspian Sea

by

Richard Frühmann

August 2005

This dissertation is submitted to the Department of Mathematics in partial fulfilment of the requirements for the degree of Master of Science.

Abstract

This project was motivated by the needs of the oil industry for improved forecasts in the central Caspian Sea. Data for the months of August 2004 to January 2005 taken from an oil rig was provided by FUGRO GEOS. The analysis of this data in conjunction with GFS-model output and Satellite images showed the severe winds to be caused by the influence of the Caucasus mountains on the general circulation rather than thermal effects of the Caspian Sea. Mechanical effects produce two distinct flow regimes during the severe wind events. In the first case the flow is simply blocked by the steep slopes of the surrounding mountains, and convergence around the tip of the Abseron Peninsula results in acceleration of the wind. The second case is related to flow channelling by the Kura Valley that separates the Greater Caucasus from the Lesser Caucasus. This explains the aegestrophic acceleration of the flow but does not adequately account for the direction of the wind at the peninsula.

Declaration

I confirm that this is my own work, and the use of all material from other sources has been properly and fully acknowledged.

Richard Frühmann

Acknowledgement

I would like to thank Dr. Robert Plant for his supervision and guidance throughout this project. His open approach towards the project allowed for stimulating discussions and a plethora of ideas. I would also like to thank Trevor Pitt not only for providing the data but more importantly for sharing his wealth of experience in forecasting for remote locations.

I would also like to express my gratitude to Dr. Adrian Dobre whose useful advice and assistance in wavelet analysis helped me overcome what appeared to be an overwhelming hurdle.

A very special thanks is due to Prof. Mike Baines whose ability and persistence at tackling students problems were most gratuitously received. His continued support, encouragement and guidance were much appreciated throughout the year.

Lastly, I would like to thank my family and friends for their love and support.

Contents

1	Introduction	2
	Structure of the Report	3
2	Literature Review	4
2.1	General Literature	4
	Lake Winds	4
	Synoptic Scale Mountain Winds	5
	Coastal Winds	6
2.2	Caspian Sea Literature	6
3	Data	8
3.1	Orography	9
3.2	Site Data	10
	Wind	10
	Pressure	12
	Temperature	13
	Humidity	14
3.3	Satellite Data	14
3.4	Model Data	15
3.5	Radiosonde Data	16
3.6	Discussion	17
4	Southerly Storms	20
4.1	Scale Analysis	21
4.2	Flow Reversal	23
5	A Simple Model of Mountain Blocking	24
5.1	Application to the Abseron Peninsula	26
6	Conclusion	30

<i>CONTENTS</i>	1
A Data Plots and Analyses	31
A.1 Wavelet Plots	31
Why Wavelets	31
Description of the Plots	32
A.2 Storm Events	38
Type 1. Events	38
Type 2. Events	41
Type 4. Events	44
B Derivation of the Stream Function	46

Chapter 1

Introduction

Mountains and lakes are known to influence atmospheric flows on all scales ranging from turbulent eddies of a few hundred meters through to Rossby waves in the global circulation. [12] Often severe winds can be induced locally in a relatively sedate mean flow. Some are regular and highly predictable, such as sea breezes, while others appear without warning.

Local winds are highly dependent on the shape of the terrain and require a high resolution grid to be captured accurately by computer models. For remote locations - that is, remote from the Western world where computer models aid accurate forecasting - there rarely exists a high resolution grid. As a result, industries which operate in such locations often struggle to get reliable forecasts.

One such region are the oil fields in the central Caspian Sea. There high mountains, in particular the Caucasus, but also the lesser Caucasus and the Elbruz ranges, significantly modify synoptic scale flows in a very complex manner. Frequent strong winds result which hazard the drilling operations but are often not captured by the global models that cover the region. [18]

This study was motivated by FUGRO GEOS, a company that provides weather forecasts for the oil industry in this region. It aims to explore several known effects in the light of a set of atmospheric measurements provided by FUGRO GEOS from one of their observing stations in the region.

Structure of the Report

To begin with it is important to investigate all the known mechanisms that lead to modified wind fields in the vicinity of mountains and lakes. An analysis of the available meteorological data in Chapter 3 will familiarise us with the local situation and highlight possible mechanisms.

Chapters 4 and 5 look more closely at two possible explanations for two distinct storm scenarios experienced off the Abseron peninsula. A simple model of flow blocking based on a model W. Dickey [4] applied to the Knob of the Brooks range in North Alaska is investigated in chapter 5.

Chapter 2

Literature Review

2.1 General Literature

Lake Winds

Large bodies of water act as good thermal capacitors because overturning in the upper layers allows heat to be advected more effectively and to greater depths than through land surfaces. Temperature contrasts between the land and water surfaces are the result.

On large lakes this can lead to a thermal high pressure centre forming over the lake during the day and a low at night. [1] On most lakes the scale of these phenomena is such that Coriolis effects are negligible and the resulting winds flow straight from the high to the low pressure.

These winds, known as lake (or land) breezes and are most common in the summer when the diurnal heating cycle is most intense. Towards the end of the summer, when the lake is at its highest temperature, the convection can be quite intense, leading to evening thunderstorms and squalls.

The situation is often intensified in the Autumn when a cold air mass moves across the warm lake. Strong temperature contrasts between the surface and the air can lead to deep convection and very vigorous storms.

In September 1996 a particularly extreme example of such a lake-effect storm occurred over Lake Huron. The combination of a slow moving low pressure system and a plunge of very cold air from Canada lead to the for-

mation of an intense cyclone that remained trapped over the lake for several days. [14] [9] The deep convection of moist air from the lake surface lead to heavy rainfall and lightning that accompanied the strong winds.

This lake-effect is well known to occur in the autumn and early winter over the Great Lakes, producing rain and snow over large regions of the North eastern USA. Such an effect over the Caspian Sea was suggested as a possible mechanism causing a tightly knit cloud vortex observed in 1963. [13]

Synoptic Scale Mountain Winds

Although large scale effects of mountains on global circulation has a significant effect on global climates, it is the synoptic and small scale effects that are of most immediate importance to local weather. [12] At these scales the most important effects are the retardation of fronts, adiabatic heating of air masses through forced ascent and flow channelling.

Two dominant categories of cross mountain flow are the Bora and the Föhn, though various regional names exist for the same phenomena in other parts of the world. These are accompanied by distinct thermal signatures. In the case of the Bora, typically a cold air mass that has moved southwards gets held up by a mountain range. The cold air, usually beneath a strong inversion either builds up behind the mountain range until it spills through gaps and valleys as a density current often only a few hundred metres deep. These winds can be localised to single valleys or spread across several hundred kilometres. [1]

The Föhn is marked by a temperature rise. Two main scenarios are observed. A moist air mass ascends over a mountain range, precipitating the moisture as it rises by forced convection. The latent heat released by condensation is the cause of the heating of the air mass. On the lee side a low pressure system forces the air down the slopes as a strong dry wind. Alternatively the approaching flow could be a high altitude flow, either across a plateau or over a colder air mass below. Adiabatic heating on descent causes the rise in temperature on the lee slope.

When a stable inversion is present on the lee side of the mountain range

the Föhn will often produce mountain waves and rotors. [12]

When the flow is parallel to the main chain of a mountain range it tends to split either side. Frictional effects of the slope cause positive vorticity anomalies on the right hand side and negative vorticity on the left hand side as the flow immediately adjacent to the slope is slowed down. This influences the development of frontal systems either side of the mountain range. [15]

Coastal Winds

Bends in a steep coastline can induce accelerations and changes in the direction of winds parallel coastal winds. The shallow water equations have been used to investigate the behaviour of the marine atmospheric boundary layer in northerly flows along the California coast. It was found that the Froude number of the flow was critical to the response of the flow as it rounded a convex bend. The strongest accelerations were observed in transcritical flows where the Froude number changes from less than 1 upstream to greater than 1 upon rounding the bend. [3]

Under other circumstances, flow reversals were observed inducing strong local changes to the pressure field. These flow reversals are associated with rapid transitions from clear to foggy conditions and changes to the structure of the marine atmospheric boundary layer. [10]

2.2 Caspian Sea Literature

The Caspian sea is the largest inland water surface in the world. It extends 1200 km from North to South with an average width of 320 km. While the northern part is very shallow with an average depth of only 6.2 m, the southern part of the lake is very deep with a mean of 325 m and a maximum depth of 1000 m. [26]

The Caspian Sea weather also shows strong gradients between the northern and southern regions in terms of the annual mean temperature, humidity and wind distributions. The North is colder and more humid compared to the South. The strongest winds are experienced in the region around the

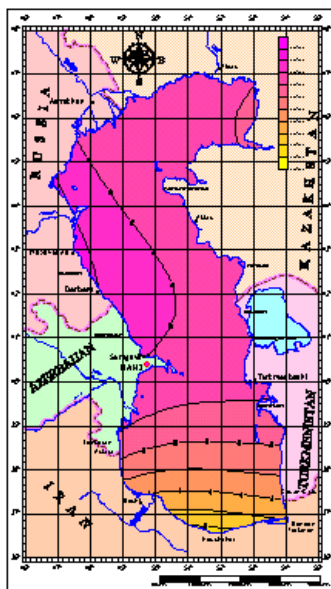


Fig 3.6 Annual wind speed above Caspian Sea

Figure 2.1: Distribution of annual mean wind strength. *Image taken from Caspian Seafacts* [21]

Abseron peninsula where they have an annual mean of $8-9 \text{ ms}^{-1}$. [21]

Due to its depth, the southern part of the lake acts as a thermal reservoir. This is seen by the mean cyclonic (anticyclonic) circulation in the winter (summer) seasons. The primary influence on the wind is through the orography which generates stationary inertial gravity and Rossby waves. [5] The dominant orographic feature in the central region are the Caucasus mountains which extend from the Black Sea to the Abseron peninsula.

Chapter 3

Data

The instable socio-economic situation in the Caspian Sea region has meant that meteorological data are scarce and records often incomplete. In compiling a picture of the region the following data were used.

Surface station records provided by FUGRO GEOS from an off-shore oil rig stationed just off the Abseron Peninsula provided minute-wise measurements of wind speed and direction, pressure, temperature and humidity for a number of periods between July 2004 and January 2005.

GFS¹ model analyses and re-analyses of sea level pressure and 500hPa geopotential height and wind speed were obtained from the website of the German Weather Center [28] and the NOAA CIRES Climatic Data Center (CDC) [22] for selected dates.

Radiosonde data was not available for nearby stations, but within a 1000km radius the archives of Wyoming University [27] contained tephigrams from a number of stations for some of the selected dates.

Visible and infra-red satellite images were obtained from the Eumetsat [25] and DISC [24] websites.

¹Global Forecasting System - the model used by the US National Oceanic and Atmospheric Administration (NOAA).

3.1 Orography

The orography around the Abseron Peninsula is dominated by the high ridge of the Caucasus Mountains which extends westwards at about 290° in an unbroken chain to the Black Sea. The highest peaks exceed 5000m and for about 800km of its length the terrain is over 2000m high.

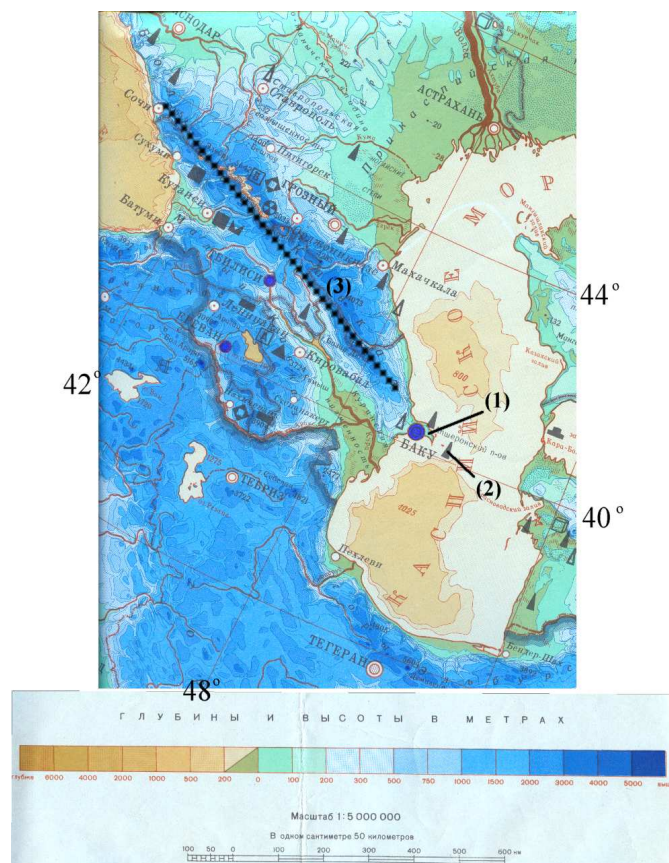


Figure 3.1: An excerpt from a Geographical map of the Soviet Union [20] showing the Caspian Sea and the Caucasus Mountains. The Abseron Peninsula (1), the approximate location of the weather station (2) and the main ridge of the Caucasus mountains (3) have been highlighted.

To the north of the Caucasus the land is flat and hardly exceeds a few hundred meters altitude all the way to the Baltic Sea. The same is true to the north and east of the Caspian Sea. The Kura river valley separates the

Greater from the Lesser Caucasus to the South. The Elbruz Mountains of northern Iran form a steep walled plateau that rings the southern part of the Caspian Sea.

3.2 Site Data

Wind

The data set included 15 near gales and gales (28 to 40 knots), and 4 severe gales (> 41 knots). The problem of distinguishing what constitutes a storm event can be seen on hand of the December plot in figure 3.2. The high frequency of winds exceeding the 28 knot threshold makes it difficult to decide where one storm ends and the next begins.

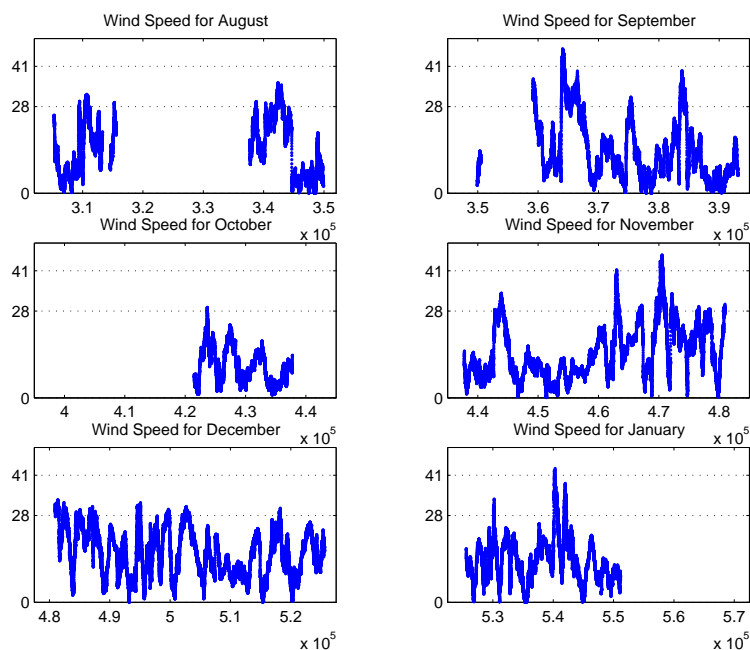


Figure 3.2: 10 minute average wind speeds (knots) for each month. The thresholds for near gale and gale have been marked to identify storm days. The time axis is in minutes $\times 10^5$ from the 1st of January 2004, 00:00.

In total 15 storms, of which 4 reached severe gale strength were identified

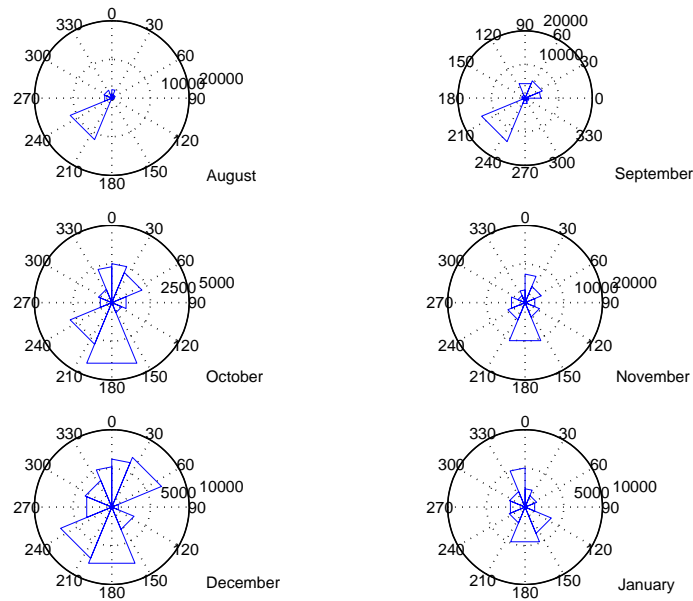


Figure 3.3: Monthly distribution of wind directions.

for analysis based on the 10 minute average wind speed. The histograms in figure 3.3 show the distribution of wind directions for each month. The tendency for the wind to come from either southerly or northerly directions is true all year round. [18]

In the early autumn the wind comes more frequently from the South. As of December there is an increase in the number of storms blowing from the North. This might be significant, distinguishing between winter and autumn storm mechanisms. Unfortunately due to gaps in the data set (only November and December have a complete record) possible trends in the monthly mean wind strength and frequency of gale force winds cannot be identified.

A wavelet analysis was performed on each months data. The storm events have strong oscillations over a large range of scales. In between some smaller scale signals can be identified at a scale of approximately 120 minutes in September, October and December. The storms of the 10th, 18th and 24th of September and 22nd of October show oscillatory behavior in the signal that grows in the days leading up to the major storm as shown in figure 3.4.

This frequency and scale were not observed in the wind direction data.

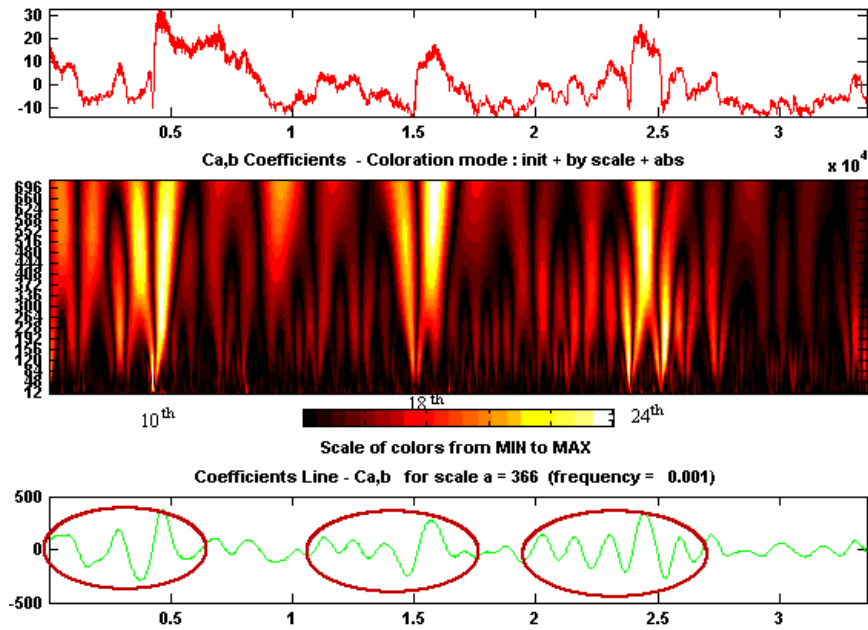


Figure 3.4: Wavelet analysis for the September 10 minute average wind speed. A series of oscillations are present that grow in the lead up to the three major storms.

The analysis was conducted on the sine of the wind direction data to avoid jumps in the signal the direction moves between 359° and 0° .

Pressure

Both the actual pressure (QFE) and the mean sea level pressure (QNH) were given in the data set. It is interesting to note that the QNH is consistently 2 hPa higher than the QFE. Since the Caspian Sea lies at 26m below mean sea level, we can deduce a station height of approximately 50m above the sea surface. Hence we might expect the wind measurements to be notably higher than the 10m winds typically calculated by numerical models.

A puzzling finding was that a wavelet analysis of the pressure curve showed distinct regular maxima at a scale of approximately 120 minutes. This corresponds to an oscillation period of approximately 8 hours. The feature is particularly evident in the signal for September shown in figure 3.5.

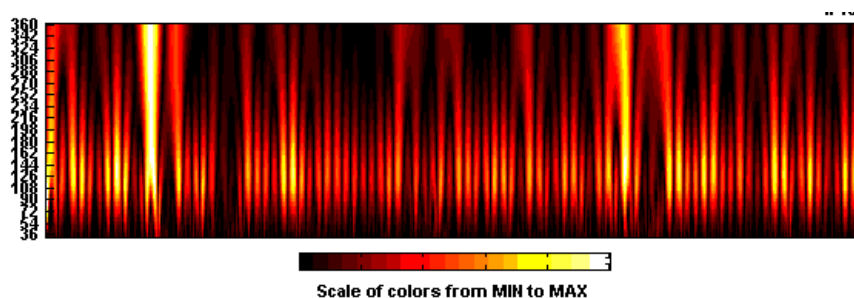


Figure 3.5: Wavelet analysis of the QNH pressure signal for September showing regular maxima approximately every hours at a scale of 120 minutes.

Two possible explanations were suggested for these pressure oscillations.

The first idea was that they result from mountain waves. These usually occur in flows perpendicular to a ridge, forming stationary waves in the lee. However, in such a flow the observation station would lie next to the ridge rather than in the wake. Parallel flows tend not to produce mountain waves since the air tends to flow around rather than over the ridge. Also, the regular occurrence of these fluctuations over very long time periods in a varying flow regime seems to make this a dubious explanation.

A second hypothesis was that they are perhaps induced by vortex shedding at the trailing edge of the mountain chain. Alternating cyclonic and anticyclonic vortices might induce local low and high pressure centers that move downstream in the wake of the obstruction, causing the observed fluctuations as they pass over the observing station. Similar oscillations were found in the wind strength but not in the wind direction.

Temperature

The temperature profiles show a strong diurnal cycle in the early autumn months, which appears to be marginally weaker during the September storms. This cycle disappears mostly as the autumn progresses. This can be ascribed in part to increased cloud cover seen on the satellite images, and to shorter days leading to weaker fluctuations.

The decrease in day length can be seen by the decrease in the scale of the

diurnal oscillation visible in the wavelet analyses. No other structures can be observed to coincide with the storms.

Humidity

In the early autumn the humidity shows a strong diurnal cycle (dry days, humid nights) varying between 40% and 80% in August with the magnitude of the oscillations decreasing towards the end of September. The mean remains fairly constant at approximately 70% all the way through to January.

No correlations to the storms was identified in either the time series or the wavelet analyses.

3.3 Satellite Data

In 1963 the TIROS VII satellite photographed a tightly knit cloud spiral over the central Caspian sea. This photo was published in the “Picture of the Month” series of the “Monthly Weather Review”, in which three possible causes were put forth.

1. “Association with a weak cold front analysed over the Caspian Sea.
2. Mechanically induced circulation caused by flow over the Caucasus mountains.
3. Thermally induced circulation caused by surface heating from the relatively warm sea.” [19]

In a detailed study, W.E Shenk [13] concludes that a well defined upper level wind circulation which remained stationary over the lake long enough to pick up sufficient water for the cloud formation is the most likely cause for the phenomenon, similar to the lake effect storms over the Great Lakes in North America.

Visible and infrared images from Meteosat 8 [25] showed no similar cyclone structures on any of the selected dates. The only significant cloud spiral

observed was for the January storm which featured a long spiral arm extending southwest over Iran. However this was related to a small low pressure over northeastern Irak rather than a thermal low induced over the Caspian Sea.

Infrared data from AIRS polar orbiting satellite [24] was obtained for several of the dates of interest. None of these showed a positive thermal contrast between the lake and the near surface air that could be likened to the "Hurricane Huron" scenario. [14] In fact the lake surface was colder than the air over most of its area. This discards the idea that surface induced thermal convection is a significant mechanism.

3.4 Model Data

Two sources were used for GFS model output data. The German weather center provides a public archive of images of analysis runs at 00Z from 1998 to the present. The maps show sea level pressure and 500 hPa geopotential height contours for the whole northern hemisphere. The three days leading up to an event and the two following it were used to gain an understanding of the evolution of the synoptic systems.

The model has a resolution of 1° over the Caspian Sea region. [28] At 40°N this makes for a 100km grid spacing. With a width of only just over 100km along its 800km length the Caucasus mountains cannot be adequately represented on such a coarse grid.

No low pressure system could be seen to move across the central Caspian Sea as suggested by the time series. Infact very little structure could be identified at this level. At the 500 hPa height however there did appear to be the trend that a trough would typically extend southwards across the Caucasus during most storms.

A finer grading of pressure contours was provided by the GFS re-analysis output from the CDC website. These revealed a recurring pattern. Typically a high pressure resides over the Black Sea extending eastwards over the Caucasus to produce a northerly or easterly geostrophic flow over the central Caspian Sea.

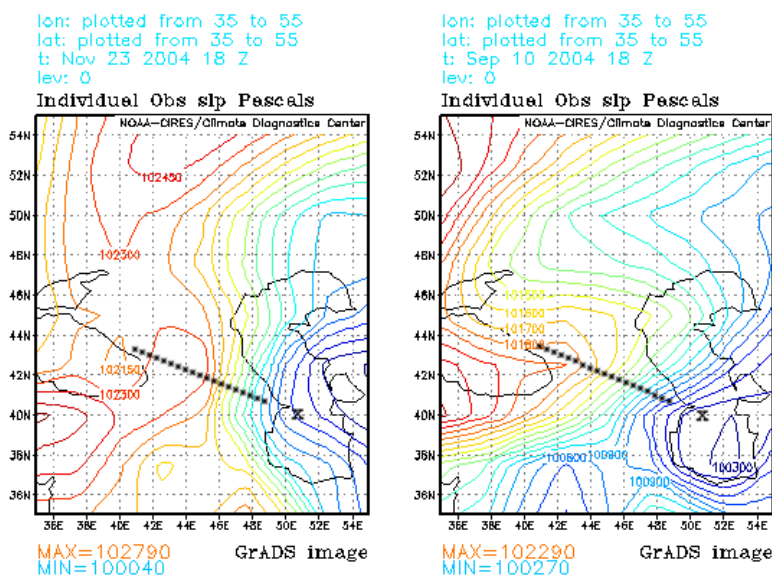


Figure 3.6: Sea level pressure plots produced by the CDC website [22]

Two distinct scenarios can be identified, both coinciding with northerly and southerly storms. Figure 3.6 depicts the case where there is a strong pressure gradient along the axis of the Caucasus mountains. Figure 3.7 depicts the case where the pressure gradient is across the mountains. The left plots are examples of southerly storms while the right plots are examples of northerly storms of the same magnitude. The axis of the main ridge of the Caucasus and the location of the weather station have been sketched in for orientation.

3.5 Radiosonde Data

Wyoming University archives hold data from a weather station at Divnoe, located 250 km north of the Caucasus at 45.9°N 43.4°E . Radiosonde ascents were found for seven of the selected dates. These showed the wind in the troposphere to come from either west- to southwesterly or north- to northeasterly directions.

The four ascents under north- and northeasterly conditions all showed

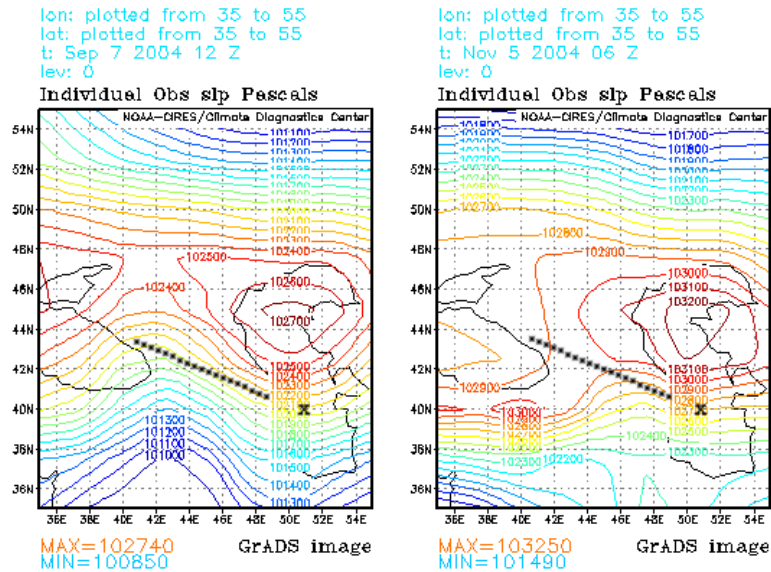


Figure 3.7: Sea level pressure plots produced by the CDC website [22]

chaotic winds with a wind shear of up 180° in the the lower 1500 m of the atmosphere and a weak or moderate inversion around 800 m. A more gradual wind shear and a moderate inversion around 1500 m was noted in the west- and southwesterly cases on the 10th and 24th of September. In all seven cases the atmosphere was stable.

A 115 knot due westerly jet was recorded at 13000 m on the 26th of October. This appears to have been completely detached from the flow in the troposphere which at 12000 m was 35 knots NNE. The upper level jet appears not to influence the lower level flow in this case.

3.6 Discussion

No distinct temperature or humidity signature in the time series suggests that the wind is not driven by either a Bora or Föhn type mechanism.

The lack of a strong thermal contrast between the lake surface and the atmosphere discards the possibility that the circulation might have a thermal low pressure at its root. (This stands in contrast to the summer situation

where it is known that a thermal low pressure, forming over the land to the east of the lake during the day, moves across the warm lake at night causing strong winds of 20 - 30 knots in the early morning hours. [18])

Hence the storms must be induced by the synoptic flow over the region. Here we can distinguish between four cases:

1. geostrophic flow from the North producing a northerly wind storm,
2. geostrophic flow from the North producing a southerly wind storm,
3. geostrophic flow from the East producing a northerly wind storm,
4. and geostrophic flow from the East producing a southerly wind storm.

The first case seems fairly straight forward. A stable atmosphere could inhibit the air from rising over the mountain chain forcing the air around the barrier. The acceleration in the wind might then be ascribed to convergence as the air flow is diverted around the edge of a barrier in the flow. This could apply to the events on the 22nd of October, 18th and 23rd of November, the 11th of January and possibly the 16th of December.

The fourth case may be caused by the same mechanism in which the easterly flow may be deflected northwards by the steep slopes of the Elbruz mountains as they curve north towards Kura river valley. There a downvalley wind might block the flow from blowing up the narrow channel between the Greater and Lesser Caucasus, thereby inducing the strong southerly winds. This would account for the storms on the 7th, 18th and 24th Septmeber.

In both these cases a stable atmosphere or strong inversion would be required to inhibit vertical motion. Unfortunately no radiosonde ascents were available from upstream stations on these dates.

The Southerly storms under Northerly geostrophic flow could be explained by flow channeling as described by J. Overland in his scale analysis of ageostrophic accelerations commonly observed in marine straights. [11] This idea will be explored in the following chapter as a possible explanation for the storms on the 10th of September, 1st, 5th and 10th of December. The two summer storms on the 4th and 26th of August weakly match this case as well.

The synoptic situation on the 5th of November fits very well to the third scenario. On closer inspection however it seems that this storm may not be caused by the large scale flow seen on the synoptic charts.

It is the only storm event which shows a distinct temperature drop over the 24 hr period of the storm. An upper level trough that extends southward over the Caucasus and the very stable, dry cold air near the surface at Divnoe are suggestive of a of polar continental air mass. A weak northerly wind is recorded at midnight on the 4th. The coldest point on the temperature curve at the oil rig coincides with the strongest wind and a sharp drop (30%) in the humidity.

It seems that this storm may be better explained as a cold flow from the North, deflected by a steep mountain barrier and accelerating around the edge as in scenario 1.

Chapter 4

Southerly Storms

In this chapter we evaluate the suggestion that the southerly storms that occur during cross-ridge synoptic flow may be caused by ageostrophic acceleration along the axis of the Kura river valley. This idea is born out of a study by J. Overland looking at winds in marine straights. [11] In his paper he lays down the basis for a scale analysis of the Boussinesq hydrostatic equations.

He establishes certain limitations to the method. Firstly it applies only to flows where the sea level pressure field is primarily externally imposed. In the lee of mountains this is governed by the internal Froude number. In Chapter 3 we establish in a qualitative manner that the storms are induced by synoptic scale pressure field. It would be nice to back this up with a calculation of the Froude numbers of the flows in the identified examples.

For this we require an upwind measurement of the geostrophic wind. This could easily be obtained from the model sea level pressure fields. We also need to calculate the Brunt Väisälä frequency (N) from equation (4.2).

$$Fr = \frac{V_a}{DN} \tag{4.1}$$

$$N = \frac{1}{2\pi} \left[g \frac{(\Gamma - \gamma)}{T} \right] \tag{4.2}$$

We can use standard values of g (acceleration of gravity) and Γ (dry

adiabatic lapse rate). However for the environmental lapse rate (γ) and the temperature (T) we would require radiosonde ascent data from the Kura valley. There are weather stations at T'bilisi and Yerevan, but unfortunately no records could be found for any of the required dates.

Secondly, the analysis is limited to straights with a width scale of 5-100 km and a length scale of 25-500 km. The valley that separates the Greater- from the Lesser Caucasus has a width of approximately 80 km, taking the separation of the 800 m contour. The valley narrows to $O(25)$ km at T'bilisi, 600 km from the Kura estuary. A steep slope leads down to the Rioni river estuary in the West. Hence the scale of the Kura valley is slightly larger than the limits suggested by J. Overland.

A third limitaitaion is that, although it may generally be applied to gaps on land, the effect of slope can have a major impact on the regional surface winds.¹ The slope of the valley to the East is on average $2.2m/km$. In the absence of evidence to the contrary, let us assume that this slope is sufficiently shallow that gravity driven flows can be ignored.

4.1 Scale Analysis

We set up our frame of reference as depicted in figure 4.1.

We require that

$$\frac{l}{L} \ll 1 \quad , \quad \delta \equiv \frac{D}{l} \ll 1 \quad (4.3)$$

J. Overland uses the Boussinesq hydrostatic system of equations in a non-dimensionalised form to evaluate the relative importance of various parameters in a cross-channel flow. He derives the along-channel and cross-channel equations of motion in the form shown in equations (4.4) and (4.5).

$$R_l \left[\frac{dv}{dt} + C'_D(u^2 + v^2)^{1/2}v \right] + u = -\frac{\partial p_0}{\partial y} - \frac{\partial p}{\partial y} \quad (4.4)$$

¹Here J. Overland refers to a paper by A. Ehrlich in the Bulletin of the American Meteorological Society. Unfortunately this paper was not available for viewing.

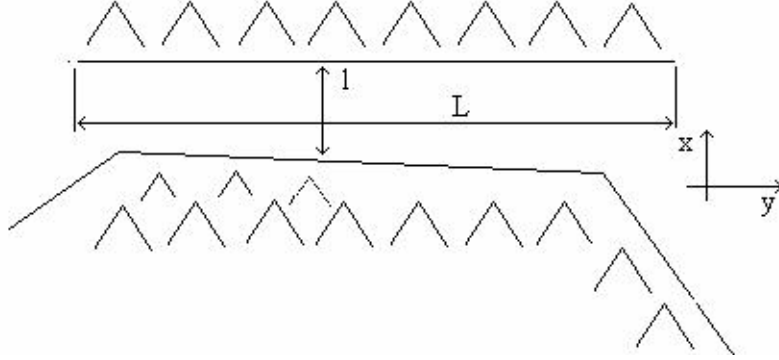


Figure 4.1: Frame of reference for the scale analysis. The height of the mountains lining the channel is assigned D .

$$R_L \left[\frac{du}{dt} + C'_D (u^2 + v^2)^{1/2} u \right] - v = -\frac{\partial p_0}{\partial x} - \frac{\partial p}{\partial x} \quad (4.5)$$

The along-channel and cross-channel Rossby numbers, R_l and R_L respectively, are measures of the nonlinearity of the momentum equations. They are given by equations (4.6) and (4.7).

$$R_l = \frac{V}{fl} \quad (4.6)$$

$$R_L = \frac{l^2}{L^2} R_l \quad (4.7)$$

C'_D is the drag coefficient for the channel. It incorporates the shear stress terms averaged over the channel height D . p_0 is the nondimensional, externally imposed pressure field and p is a small perturbation therein. The u and v velocities are in the x and y directions respectively and t is the nondimensional time.

Equations (4.4) and (4.5) have two competing terms - the geostrophic velocities u and v and the ageostrophic terms in brackets. When R_l or R_L are small, then the flow will be essentially geostrophic. When they are large, then the ageostrophic acceleration perpendicular to the geostrophic flow becomes significant.

Because L is always much larger than l (equation (4.3)) R_L will always be

very small. Hence when the flow is parrallel to the channel it will be largely geostrophic. (Note that in this case $u \approx 0$ so the second term in the brackets is also very small.)

In the case where the flow is perpendicular to the mountains however we might expect to find a strong along channel acceleration, provided V is large enough that $R_l > 1$. Looking at the dimensions of the Caucasus, we find that this requires V to be at least $8\text{-}10\text{ms}^{-1}$. We see from Table 4.1 that this applies weakly to the winter scenarios but not to the two summer storms in August.

Table 4.1

Date	04/08	26/08	10/09	01/12	04/12	10/12
Geostrophic Wind ^a ms^{-1}	5	4	18.5	13.5	17.5	9.5
v ms^{-1}	4	3.5	17	8	9	9
R_l	0.53	0.48	2.13	0.98	1.14	1.10

^aFor this calculation a reference temperature was taken from the oil rig.

4.2 Flow Reversal

We see from the scale analysis that the cross mountain flow is only strong enough in on the 10th of September to produce really significant ageostrophic acceleration in the along-channel direction. In the three December cases there is already a substantial along channel component to the flow with the wind coming from 320° to 340° . Hence a smaller ageostrophic acceleration will result in a significant storm.

However this does not answer the question “why does the wind veer northwards when it exits the channel into the north- to northwesterly flow?”

One possible explanation might be found in studies of the Northerly winds along the California coast. Here flow reversals are frequently observed at sharp bends in the coastline. [10] It is possible that similar circulations occur around the Abseron pennisula. This would also help to explain the sharp change in direction from northerly to southerly observed in the data.

Chapter 5

A Simple Model of Mountain Blocking

In his paper W.Dickey [4] looks at flow around the Knob of the Brooks range in northern Alaska. By representing the mountain outcropping as a simple cylinder blocking an ideal fluid flow he is able to replicate the strength and direction of wind storms experienced at several observing stations along the coast to the north of the mountains.

Although not all the assumptions made in the model are equally applicable at lower latitudes, it was thought to be interesting to experiment with the same idea to produce a simple model of the effect of the Caucasus mountains on the northerly wind storms off the Abseron Peninsula.

In his model W. Dickey makes the following five assumptions:

1. Horizontal, two dimensional flow - this is justifiable if there is a strong inversion at some height relative to the mountains such that vertical motion over the mountains is suppressed. The choice of the elevation contour used depends on the height of the inversion in the upstream flow.
2. Constant Coriolis force - at high latitudes this is a reasonable assumption. It is less appropriate at 44°N but we can accept it if the flow does not extend across many degrees of latitude.

3. The friction force is proportional to the velocity - this is justified solely on the basis that it simplifies the equations.
4. Non-divergent flow - can only be justified by the results.
5. The flow has zero relative vorticity as it approaches the barrier - again only to be justified by the results.

In his paper he shows that assumptions 1-4 lead to a simplified form of the vorticity equation. Application of assumption 5 then leads to the stream function satisfying Laplace's equation

$$\nabla^2\varphi = 0 \tag{5.1}$$

The general 2π periodic solution of equation (5.1) can be shown to be ¹

$$\varphi(r, \theta) = \sum_{n=1}^{\infty} (a_n r^n + b_n r^{-n})(A_n \cos n\theta + B_n \sin n\theta) \tag{5.2}$$

We place a circle of radius a into the freestream flow. Applying the boundary conditions that no flow can pass through the surface of the obstacle ($\frac{\partial\varphi}{\partial r}\Big|_{r=a} = 0$) and the free stream velocity is unaffected by the obstacle ($\varphi(\infty) = Uy = U \sin \theta$) we can reduce equation (5.2) to¹

$$\varphi(r, \theta) = U \left(r + \frac{a^2}{r} \right) \sin \theta \tag{5.3}$$

where a is the radius of the circle. The velocity fields can then be calculated from the stream function by

$$(u, v) = \left(\frac{-1}{r} \frac{\partial\varphi}{\partial\theta}, \frac{\partial\varphi}{\partial r} \right)$$

giving

$$\mathbf{u} = U \left(1 - \frac{a^2}{r^2} \right) \cos \theta \tag{5.4}$$

¹See appendix B for the derivation.

$$\mathbf{v} = -U \left(1 + \frac{a^2}{r^2} \right) \sin \theta \quad (5.5)$$

With this very simple model, Dickey is able replicate the distribution of wind strength and direction and the pressure distribution along the stretch of coast in the vicinity of the Knob of the Brooks Range with some accuracy.

5.1 Application to the Abseron Peninsula

As the land to the North of the Caucasus range is very flat it may be assumed that the flow will be relatively unperturbed and therefore near geostrophic. When the synoptic scale flow is from the North, or when there is a shallow northerly current of cold air near the surface as on the 4th of November, it may be possible that the Caucasus mountains could be modeled in a similar manner.

In contrast to the Knob of the Brooks range in North Alaska, the Caucasus form a narrow ridge which would be better approximated as an ellipse with a high aspect ratio. For this we can use a Joukowski transformation (5.7) to map the circle in the z -plane to an ellipse in the ζ -plane. [16]

We can define an ellipse which approximates a chosen height contour by selecting appropriate values for A and B in equation (5.6).

$$\zeta = A \cos \theta + iB \sin \theta \quad (5.6)$$

We then map the circle $z = re^{i\theta}$ into the ζ -plane.

$$\zeta = z + \frac{c}{z} \quad (5.7)$$

$$\begin{aligned} &= re^{i\theta} + \frac{ce^{-i\theta}}{r} \\ &= \left(r + \frac{c}{r} \right) \cos \theta + i \left(r - \frac{c}{r} \right) \sin \theta \end{aligned} \quad (5.8)$$

From equation (5.8) we can now relate r , c , A and B by

$$r = \frac{1}{2}(A + B) \quad , \quad c = \frac{1}{4}(A^2 - B^2) \quad (5.9)$$

Because the ellipse is not symmetrical in all directions, we need to account for the incident angle of the freestream flow. We can now write the complex potential w as

$$w = \phi(z) + i\varphi(z) = -Uze^{i\alpha}$$

where $\phi(z)$ is the velocity potential, $\varphi(z)$ is the stream function, U is the freestream flow speed and α is the angle of the flow. Adding a circle of radius r to the flow gives

$$w = -Ue^{i\alpha} \left(z + \frac{r^2}{z} \right)$$

Finally we map w into the ζ -plane in which we have represented our ellipsoidal mountain using equation the Joukowski transformation (5.7). We wish to know the velocity components \mathbf{u} and \mathbf{v} which are the real and imaginary parts of $\frac{\partial w}{\partial \zeta}$ respectively.

$$-\mathbf{u} + i\mathbf{v} = \frac{dw}{d\zeta} = \frac{dw}{dz} \frac{dz}{d\zeta} = \frac{-Ue^{i\alpha} \left(1 - \frac{r^2}{z^2} \right)}{1 - \frac{c}{z^2}} \quad (5.10)$$

The algorithm for solving the fluid flow is now very simple. We need only to define the geometry of the idealised mountain and the direction and magnitude of the freestream flow and we can work out the velocity at any point (σ, τ) in the ζ -plane.

The difficulty is mapping our desired σ and τ to the corresponding x and y co-ordinates that we require to solve (5.10). From the Joukowski transformation we know that

$$\zeta = z + \frac{c}{z}$$

One approach is to turn this into a quadratic equation from which to solve for x and y .

$$\begin{aligned} \zeta z^2 - \zeta z + c &= 0 \\ x + iy &= \frac{\zeta \pm \sqrt{\zeta^2 - 4c}}{2} \end{aligned} \quad (5.11)$$

Taking only the positive solution we can then separate the real and imag-

inary parts within the square root by defining two variables C and D such that

$$\sqrt{(\sigma + i\tau)^2 - 4c} = C + iD$$

Squaring both sides and separating the real from the imaginary gives

$$\sigma^2 - \tau^2 - 4c = C^2 - D^2 \tag{5.12}$$

$$\sigma\tau = CD \tag{5.13}$$

Substituting $C = \frac{\sigma\tau}{D}$ in (5.12) gives

$$(\sigma^2 - \tau^2 - 4c) - \left(\frac{\sigma\tau}{D}\right)^2 + D^2 = 0$$

$$D^2 = \frac{-(\sigma^2 - \tau^2 - 4c) \pm \sqrt{(\sigma^2 - \tau^2 - 4c)^2 + 4(\sigma\tau)^2}}{2}$$

We can now substitute for D in (5.13)

$$C = \pm \left(\frac{2}{-(\sigma^2 - \tau^2 - 4c) \pm \sqrt{(\sigma^2 - \tau^2 - 4c)^2 + 4(\sigma\tau)^2}} \right)^{1/2} (\sigma\tau)$$

This gives us four possible solutions for x and y of the form

$$x = \frac{\sigma + C}{2}, \quad y = \frac{\tau + D}{2} \tag{5.14}$$

We must now decided which of the solutions gives the correct transformation for a real situation.

An alternative method starting from (5.15) was also attempted.

$$\sigma + i\tau = x + iy + \frac{c}{x + iy} \tag{5.15}$$

We can easily separate out the real from the imaginary part on the right hand side by eliminating the complex number in the denominator as follows

$$\sigma + i\tau = x + iy + \frac{c(x - iy)}{x^2 + y^2}$$

$$= \frac{x(x^2 + y^2 - c)}{x^2 + y^2} + \frac{iy(x^2 + y^2 - c)}{x^2 + y^2} \quad (5.16)$$

but are now left with the difficult task of solving for x and y in terms of σ and τ . Within the time limit of the project no solution was found.

A simple alternative is to select x and y co-ordinates around the circle in the z -plane and then transform these using the simple equation (5.16) to get the value at the corresponding point in the ζ -plane.

This is not a very satisfactory solution as we are not interested in the general flow field around an ellipse, but whether or not the flow at a particular point relative to our idealised ridge accurately represents the real flow at that point under given upwind conditions.

The next stage would be to experiment with varying the dimensions of the ellipsoid to establish a good fit with the observations. One could then proceed by adding vorticity to the flow and possibly dynamics. Unfortunately time ran out.

Chapter 6

Conclusion

Two distinct scenarios have been identified for the severe autumn and winter winds in the central Caspian Sea. These explanations are applicable to the autumn and winter months only.

Flow blocking by the Caucasus mountains appears to account for about 60% of the storms in the region. Stable atmospheric conditions inhibit vertical motion and force the flow around the edge of the mountain barrier. This leads to convergence and acceleration around the Abseron Peninsula. Depending on the direction of the approaching flow this can lead to either northerly (most common) or southerly storms of 30-40 knots.

In the second case, there appears to be channelling of cross mountain geostrophic flows in the Kura valley. Density driven flows in the valley might be accountable for the direction of the ageostrophic acceleration. The reason for the winds turning north rather than south has not been properly explored.

The primary problem in forecasting these events is likely to be one of model resolution in the region. The sharp ridge of the Caucasus is impossible to resolve on the typical grid of global atmospheric models. Another difficulty made obvious during this study is the sparsity of data in the region. Especially when trying to resolve small scale events, high resolution data is essential.

A quantitative investigation into the two mechanisms briefly outlined in this paper would be necessary to draw more confident conclusions.

Appendix A

Data Plots and Analyses

A.1 Wavelet Plots

Why Wavelets

Wavelet theory has its roots in Fourier transforms. The major difference is that in wavelet analysis one compares the signal with a finite wave shape (known as the ‘mother’ wavelet) over a range of scales rather than an infinite sine or cosine wave. [6]

Thus the wavelet analysis is able to resolve both scale and time, thereby allowing one to search for the occurrence of unique events within a signal. The scale is analogous to frequency in the Fourier transform. For instance, a mexican hat wavelet¹ would transform a sine wave into regularly occurring maxima and minima at a scale of 1/4 the period. [8] A signal with varying frequency would appear as irregular maxima and minima at varying scales. This allows one to gain more information about an irregular signal than would be obtained from a Fourier analysis.

Wavelet transforms also have numerous applications in data compression. [6] Discrete transforms are typically used for such applications.

De-noising and recognition of self-similar behaviour in a time series signal make wavelet methods interesting to signal analysis. For this the continuous

¹The second derivative of the Gaussian probability density function is commonly referred to as the mexican hat wavelet in the context of wavelet analysis.

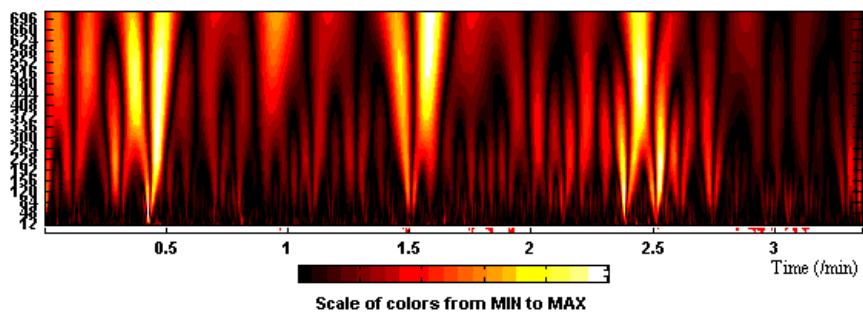
wavelet transform is most applicable. [17] A popular choice is the mexican hat wavelet since it's strong localisation in time makes it idea for identifying singular events. Higher order derivatives of the gaussian wavelet can be used if one is looking for small wave groups.

Description of the Plots

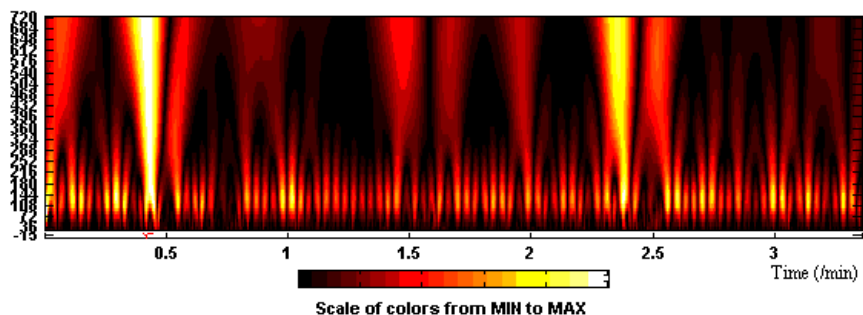
The plots displayed here were generated using the 1D-continuous transform in the Matlab 'wavelet toolbox'. A mexican hat wavelet was used to analyse the signals over a range of scales from 36 - 720 minutes in intervals of 12 minutes.

The time axis is in minutes from the start of the signal. Not all signals start on the 1st day of the corresponding month. The analyses for August have been ommitted from this section for reasons of organisation of the presentation. The storms can be identified on the basis of the windspeed and pressure plots.

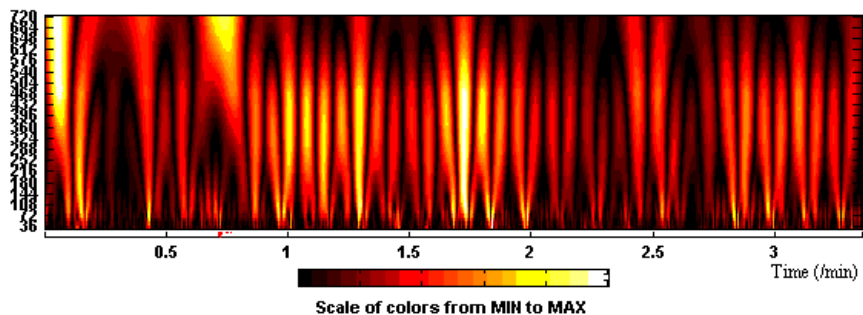
It should be noted that wind speed measurements are missing from the October plot. As storm events were identified on the basis of the wind speed, there may be some storm occurences that have not been identified in the corresponding pressure, temperature and humiditiy signals.



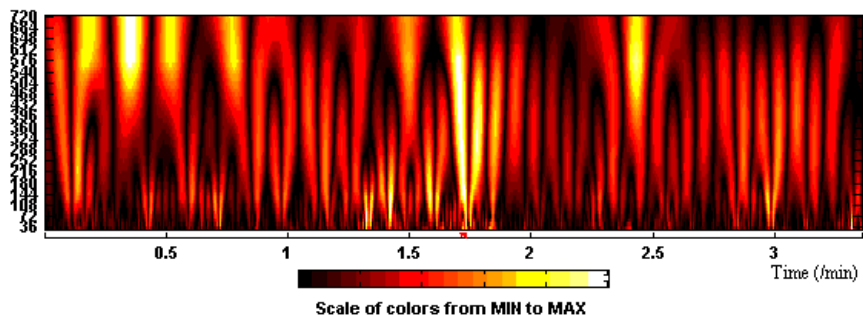
(a) Wind Speed (10 minute average)



(b) QNH Pressure (10 minute average)

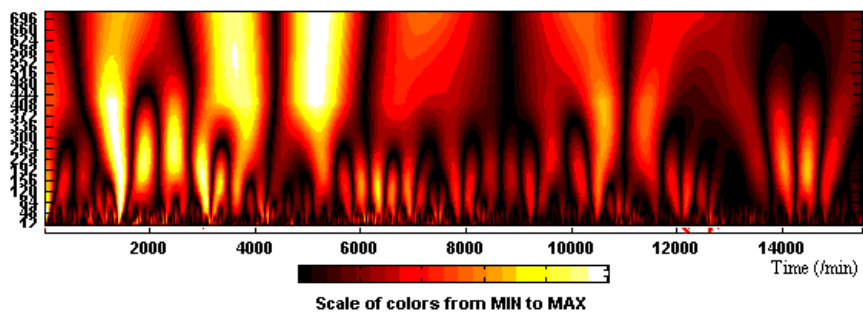


(c) Temperature (10 minute average)

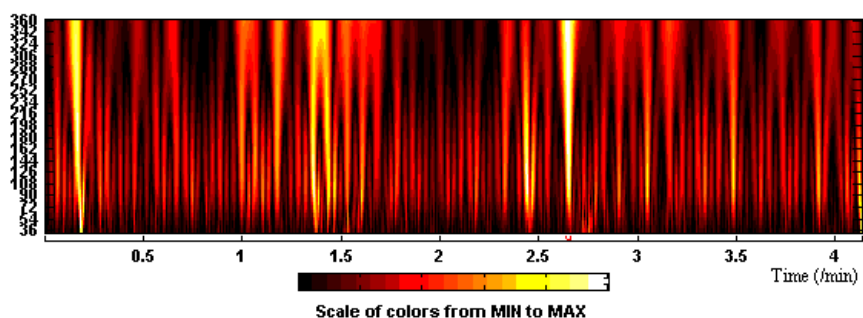


(d) Relative Humidity (10 minute average)

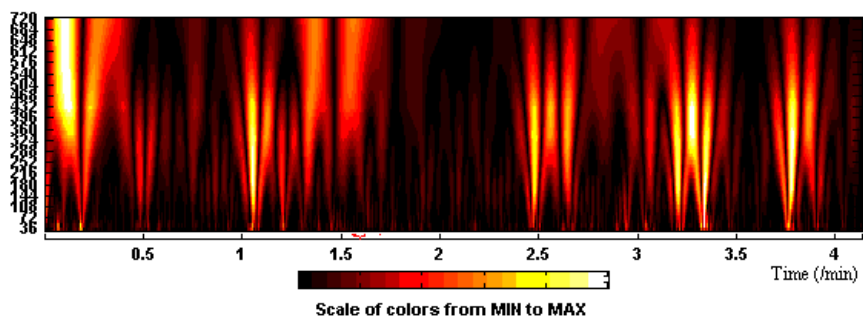
Figure A.1: Wavelet analysis for the month of September



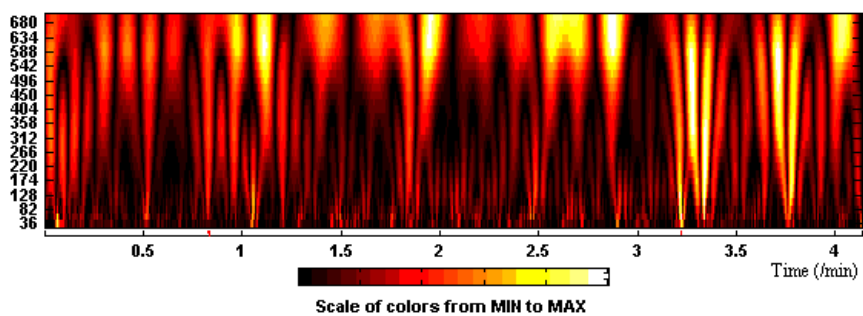
(a) Wind Speed (10 minute average)



(b) QNH Pressure (10 minute average)

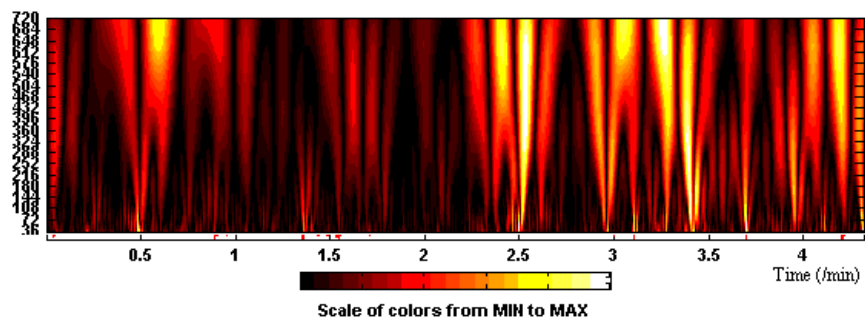


(c) Temperature (10 minute average)

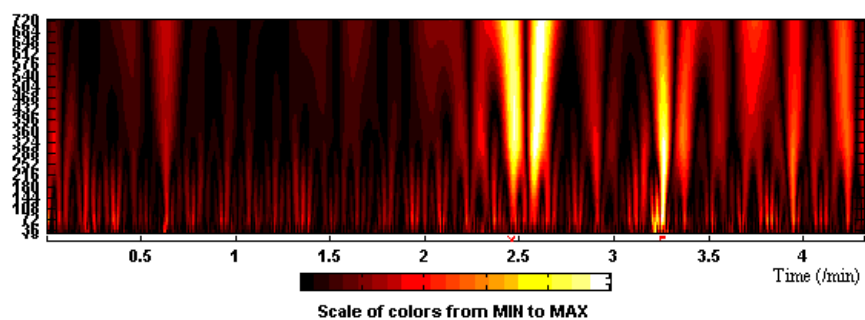


(d) Relative Humidity (10 minute average)

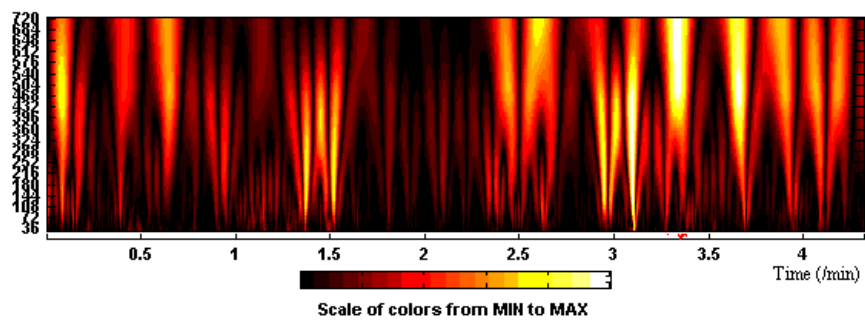
Figure A.2: Wavelet analysis for the month of October



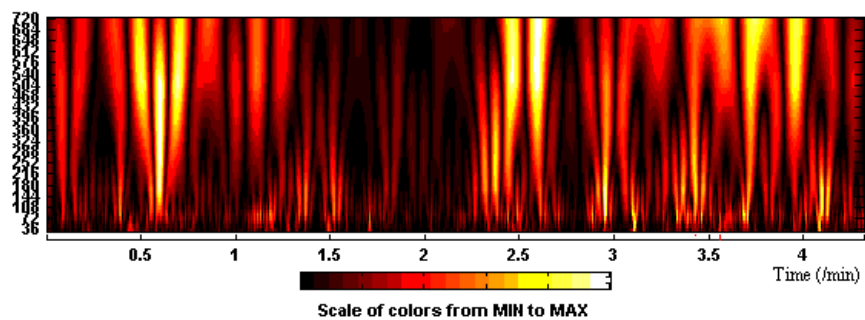
(a) Wind Speed (10 minute average)



(b) QNH Pressure (10 minute average)

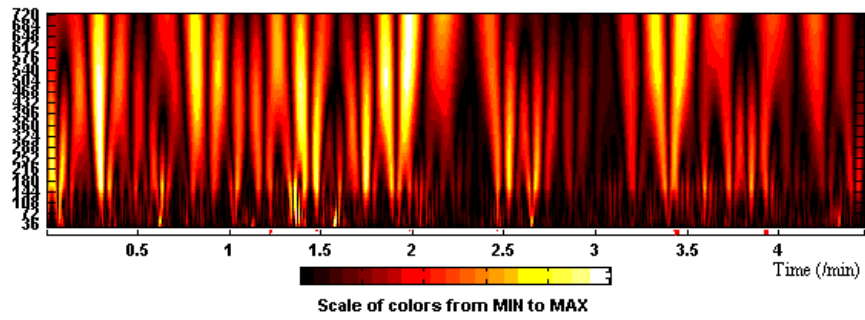


(c) Temperature (10 minute average)

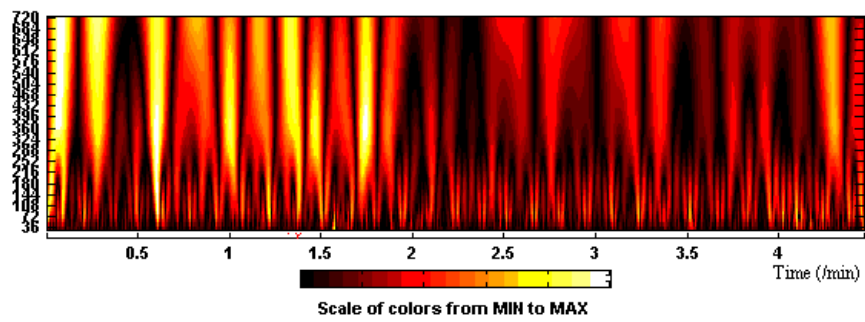


(d) Relative Humidity (10 minute average)

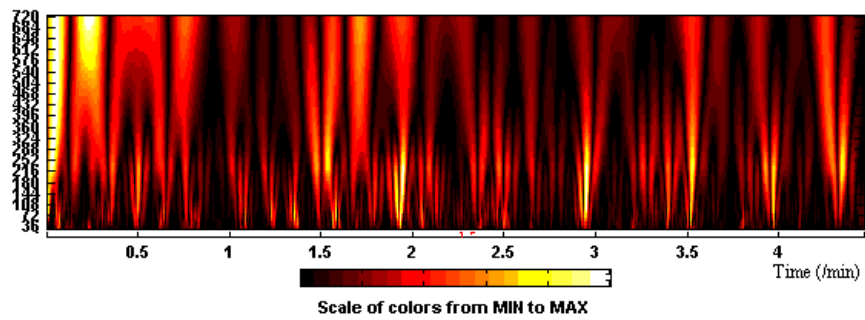
Figure A.3: Wavelet analysis for the month of November



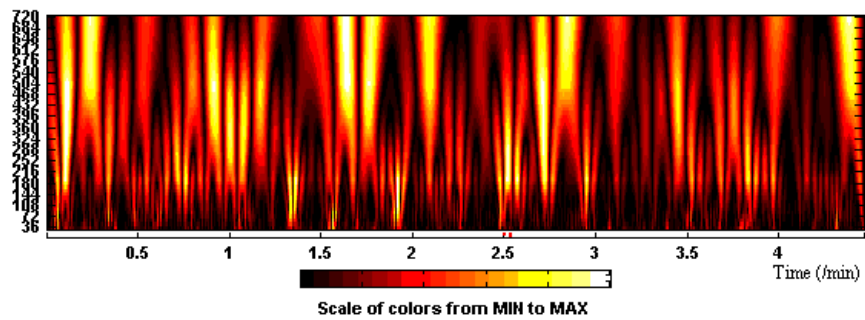
(a) Wind Speed (10 minute average)



(b) QNH Pressure (10 minute average)

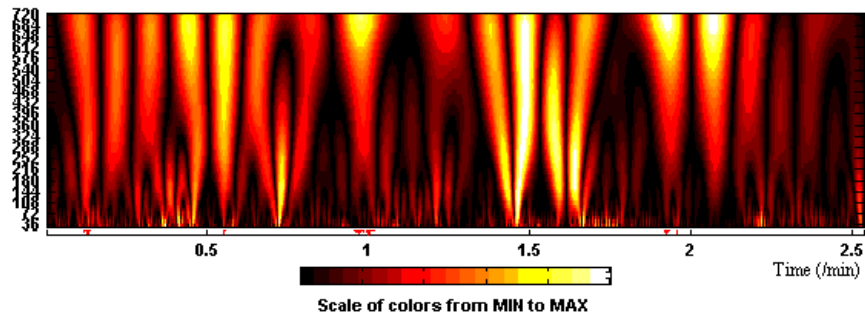


(c) Temperature (10 minute average)

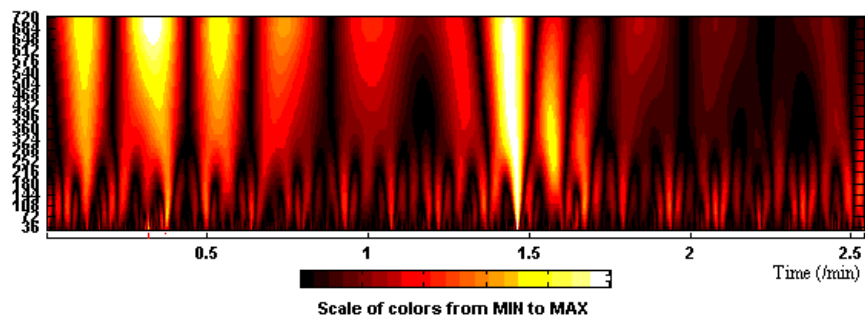


(d) Relative Humidity (10 minute average)

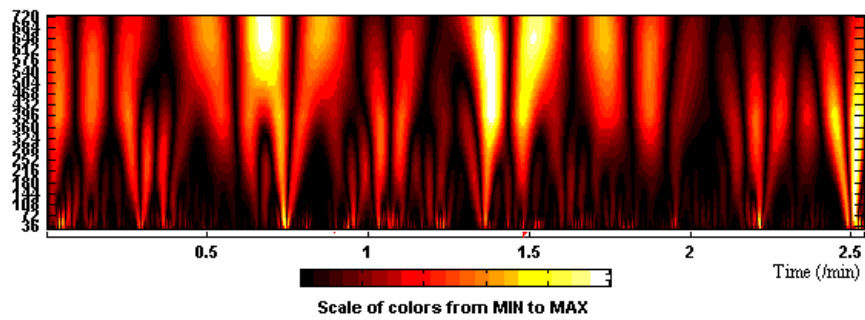
Figure A.4: Wavelet analysis for the month of December



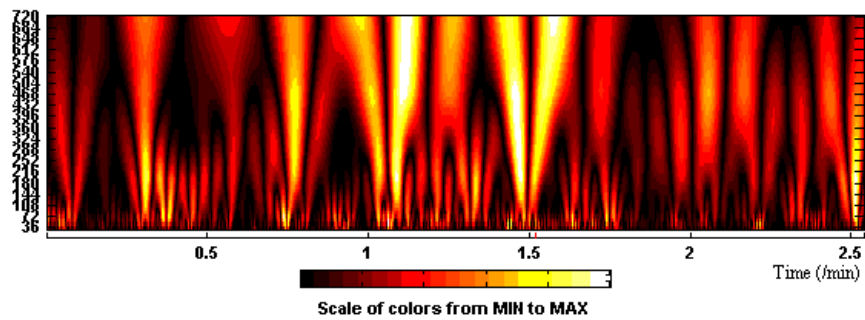
(a) Wind Speed (10 minute average)



(b) QNH Pressure (10 minute average)



(c) Temperature (10 minute average)



(d) Relative Humidity (10 minute average)

Figure A.5: Wavelet analysis for the month of January

A.2 Storm Events

The following plots are 5 day time series centered about the identified storms. These try to show the correlation between windspeed, pressure, temperature and humidity tendencies. They have been grouped in the categories defined in section 3.6 rather than placed in chronological order.

Type 1. Events

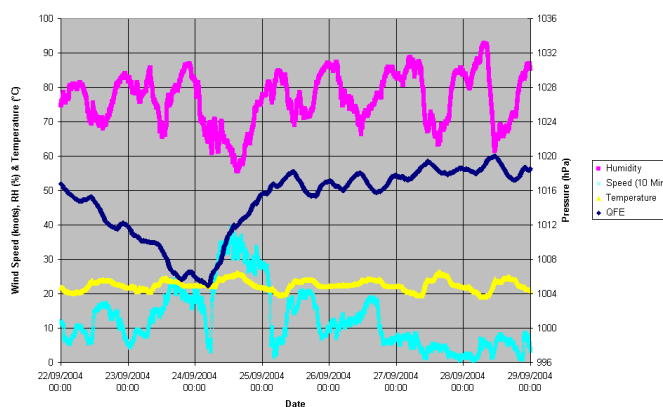


Figure A.6: Time series for the 22nd of October 2004 near gale.

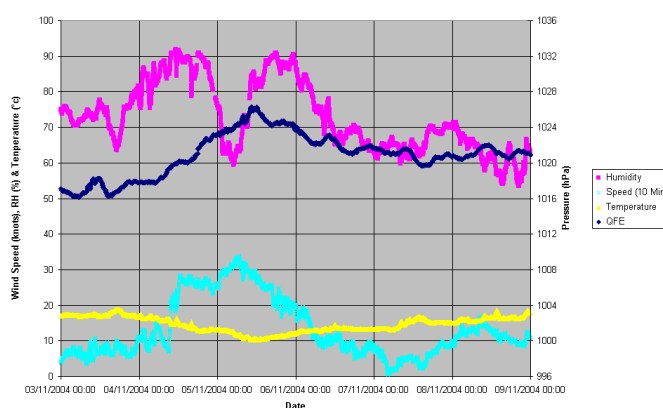


Figure A.7: Time series for the 5th of November 2004 gale.

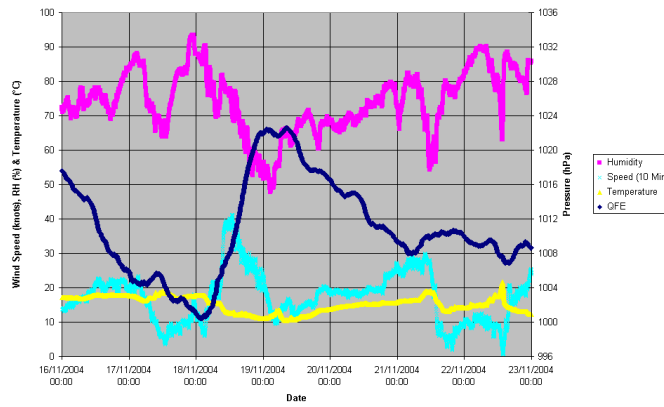


Figure A.8: Time series for the 18th of November 2004 severe gale.

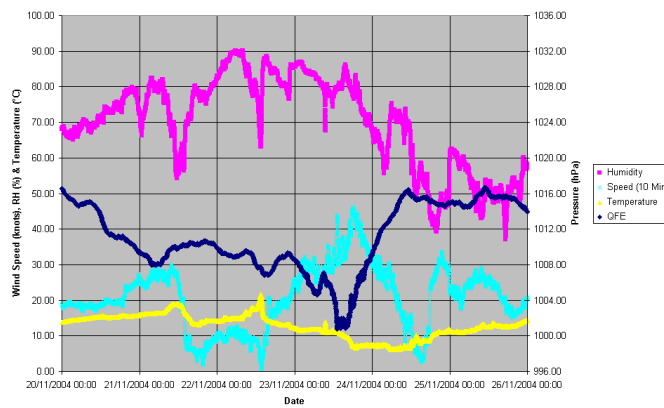


Figure A.9: Time series for the 23rd of November 2004 severe gale.

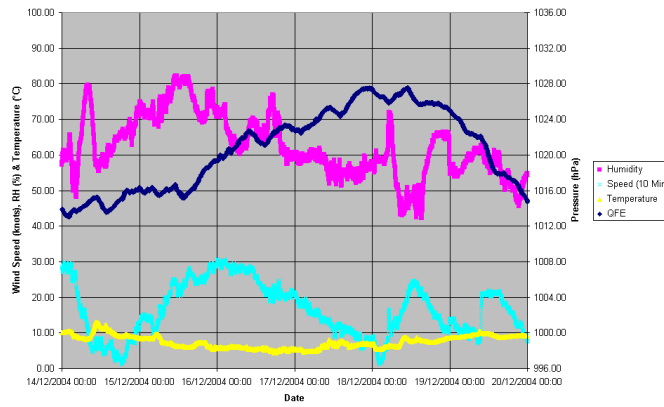


Figure A.10: Time series for the 16th of December 2004 gale.

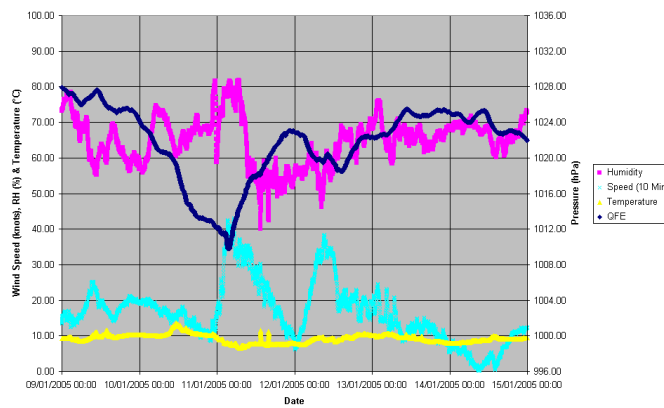


Figure A.11: Time series for the 11th of January 2005 severe gale.

Type 2. Events

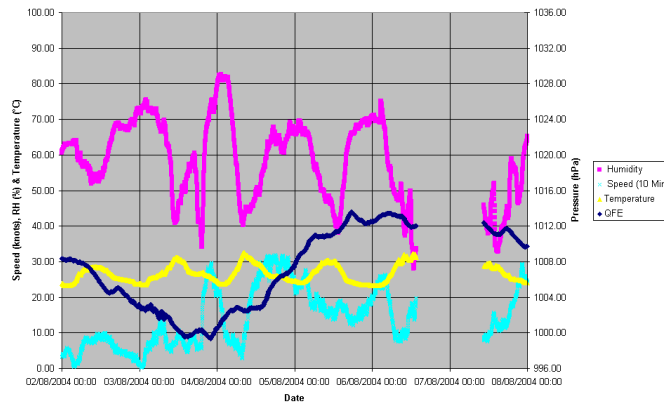


Figure A.12: Time series for the 4th of August 2004 gale.

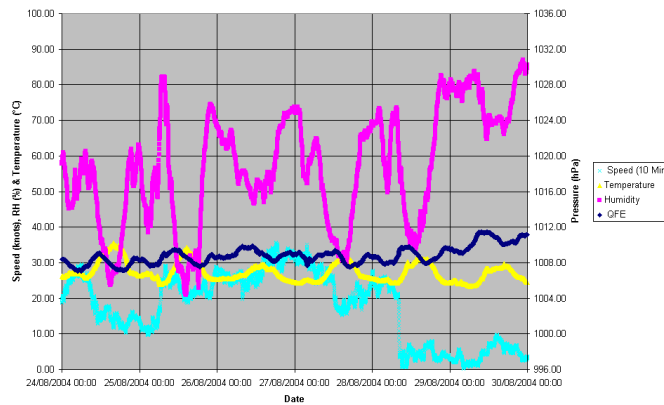


Figure A.13: Time series for the 26th of August 2004 gale.

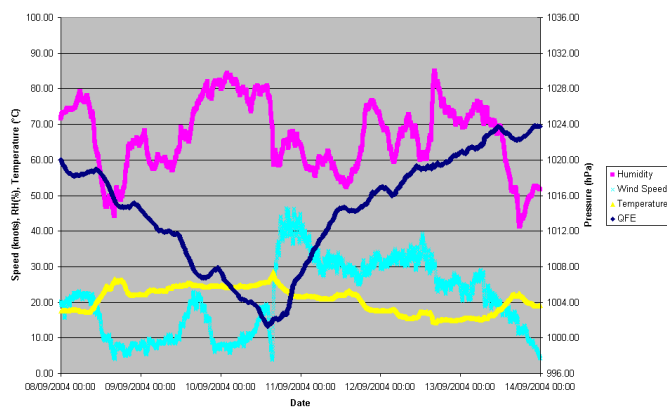


Figure A.14: Time series for the 10th of September 2004 severe gale.

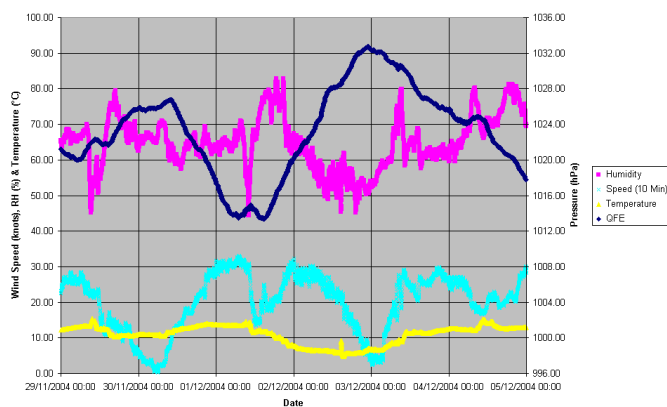


Figure A.15: Time series for the 1st of December 2004 near gale.

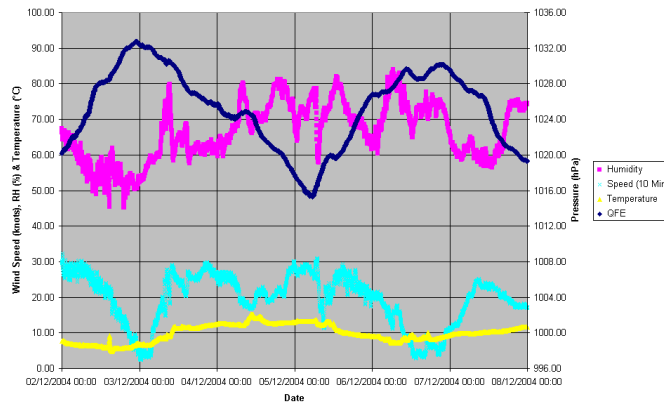


Figure A.16: Time series for the 4th of December 2004 near gale.

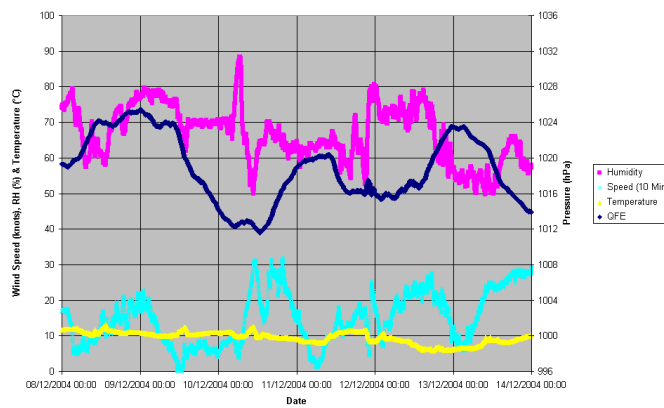


Figure A.17: Time series for the 10th of December 2004 near gale.

Type 4. Events

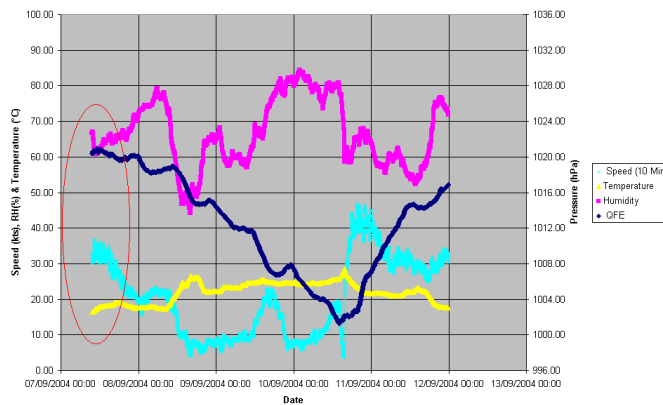


Figure A.18: Time series for the 7th of September 2004 gale.

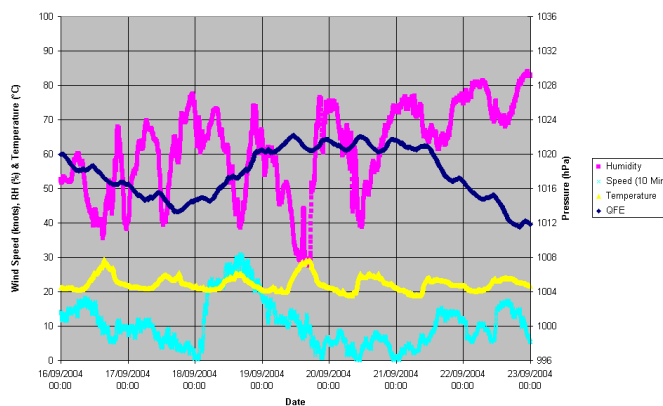


Figure A.19: Time series for the 18th of September 2004 gale.

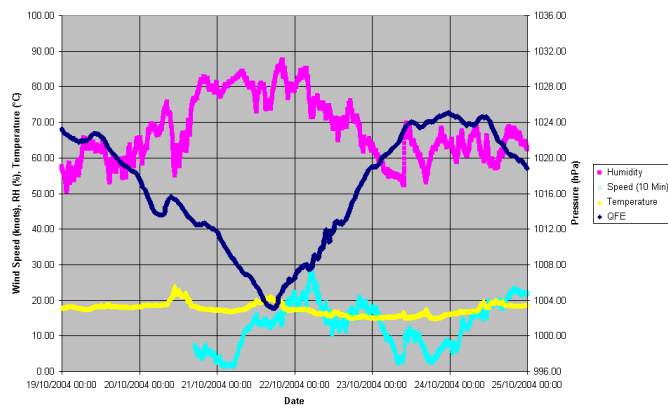


Figure A.20: Time series for the 24th of September 2004 severe gale.

Appendix B

Derivation of the Stream Function

We begin with Laplace's equation written in polar co-ordinates.

$$\frac{\partial^2 \Phi}{\partial r^2} + \frac{1}{r} \frac{\partial \Phi}{\partial r} + \frac{\partial^2 \Phi}{\partial \theta^2} = 0 \quad (\text{B.1})$$

We assume that there exist two functions $R(r)$ and $\Theta(\theta)$ such that

$$\Phi(r, \theta) = R(r)\Theta(\theta) \quad (\text{B.2})$$

We can then rewrite equation (B.1) as

$$\begin{aligned} \Theta \ddot{R} + \Theta \frac{1}{r} \dot{R} + R \frac{1}{r^2} \ddot{\Theta} &= 0 \\ \frac{r^2}{R} \left(\ddot{R} + \frac{\dot{R}}{r} \right) &= -\frac{\ddot{\Theta}}{\Theta} = \alpha \end{aligned} \quad (\text{B.3})$$

Setting $\alpha = \lambda^2 \geq 0$ we can solve for a periodic solution in θ .

$$\ddot{\Theta} + \lambda^2 \Theta = 0$$

therefore

$$\Theta = A \cos \lambda \theta + B \sin \lambda \theta \quad (\text{B.4})$$

is a 2π periodic solution where λ is an integer. We can solve for R by substitution.

$$r^2\ddot{R} + r\dot{R} - \lambda^2 = 0$$

If we let $R = r^\gamma$ we can write

$$\begin{aligned} r^2(\gamma(\gamma - 1)r^{\lambda-2}) + r(\lambda r^{\lambda-1}) - \lambda^2 r^\gamma &= 0 \\ (\gamma(\gamma - 1)) + \gamma - \lambda^2 &= 0 \end{aligned}$$

so either $r = 0$ or $\gamma^2 - \lambda^2 = 0$. Ignoring the case where the radius is zero, we get

$$R = ar^\lambda + br^{-\lambda} \quad (\text{B.5})$$

This gives us the general solution

$$\Phi(r, \theta) = \sum_{n=1}^{\infty} (a_n r^n + b_n r^{-n})(A_n \cos \lambda\theta + B_n \sin \lambda\theta) \quad (\text{B.6})$$

We can simplify this solution for the case flow around a circle. If we separate the term where $n = 1$ from the terms where $n \geq 2$ we find that the boundary conditions at the surface ($\frac{\partial\varphi}{\partial r}\big|_{r=a} = 0$) and at infinity ($\varphi(\infty) = Uy = U \sin\theta$) lead to

$$\begin{aligned} a_1 B_1 &= U \quad , \quad A_1 = 0 \\ a_n &= b_n = 0 \quad \text{for all } n \geq 2 \\ \frac{b_1}{a_1} &= a^2 \end{aligned}$$

Hence equation (B.6) simplifies to

$$\Phi(r, \theta) = U \left(r + \frac{a^2}{r} \right) \sin \theta \quad (\text{B.7})$$

Bibliography

- [1] C.D.Ahrens, 2000, "Meteorology Today: an Introduction to Weather, Climate and the Environment, *6th Edition*", *Brookes/Cole*
- [2] G.D. Bell, L.F. Bosart, 1989, "A 15-yr. Climatology of Northern Hemisphere 500mb Closed Cyclone and Anticyclone Centers", *Monthly Weather Review*, *Vol.117 pp.2141-2163*
- [3] S. Burk, T. Haack, R. Samelson, 1999, "Mesoscale Simulation of Supercritical, Subcritical and Transcritical Flow along Coastal Topography", *Journal of the Atmospheric Sciences*, *Vol.56 pp.2780-2795*
- [4] W.W. Dickey, 1961, "A Study of a Topographic Effect on Wind in the Arctic", *Journal of Meteorology*, *Vol. 18 pp.790-803*
- [5] V.V. Efimov, M.V. Shokurov, V.S. Barabanov, 2002, "Physical Mechanisms of Wind Circulation Forcing over the Inland Seas", *Izvestiya, Atmospheric and Oceanic Physics*, *Vol.38 No.2 pp.217-227*, Translated by B. Dribniskaya
- [6] A. Graps, 1995, "An Introduction to Wavelets", *IEEE Computational Science and Engineering*, *Vol.2 num.2*
- [7] V.M. Karyampudi, S.E. Koch, C. Chen, J.W. Rottman, M.L. Kaplan, 1995, "The Influence of the Rocky Mountains on the 12-14 April 1986 Severe Weather Outbreak. Part II: Evolution of a Prefrontal Bore and Its Role in Triggering a Squall Line", *Monthly Weather Review*, *vol.123 pp.1423-1446*

- [8] J. Lewalle, 1998, "Wavelets without Lemmmas: Part I of a 2-part Lecture Series on Applications of Continuous Wavelets to Data Analysis", prepared for the VKI Lecture Series April 6-8, 1998, Syracuse University, <http://www.mame.syr.edu/faculty/lewalle>
- [9] T. Miner, P. Sousounis, J. Wallman, G. Mann, 2000, "Hurricane Huron", *Bulletin of the American Meteorological Society*, Vol.81 pp.223-236
- [10] W. Nuss, J. Bane, W. Thompson, T. Holt, C. Dorman, F. Ralph, R. Rotunno, J. Klemp, W. Skamarock, R. Samelson, A. Rogerson, C. Reason, P. Jackson, 2000, "Coastally Trapped Wind Reversals: Progress Toward Understanding", *Bulletin of the American Meteorological Society*, Vol.81 pp.719-743
- [11] J.E. Overland, 1984, "Scale Analysis of Marine Winds in Straights and along Mountainous Coasts", *Monthly Weather Review*, vol.112 pp.2530-2534
- [12] B.G. Roger, 1992, "Mountain Weather and Climate, 2nd edition", *Routledge (London)*
- [13] W.E. Shenk, 1965, "Analysis of a Caspian Sea Vortex" *Monthly Weather Review*, vol.93 pp.613-617
- [14] P.J. Sousounis, J. Wallman, G.E. Mann, 2001, "Hurricane Huron': An Example of an Extreme Lake-Aggregate Effect in Autumn", *Monthly Weather Review*, vol.129 pp.401-419
- [15] A.J. Thorpe, H. Volkert, D. Heimann, 1992, "Potential Vorticity of Flow Along the Alps", *Joint Centre for Mesoscale Meteorology, Internal Report 12*
- [16] Prof. Mike Baines, Reading University
(*personal communication*)
- [17] Dr. Adrian Dobre, Reading University *personal communication*
- [18] Trevor Pitt, senior forecaster at FUGRO GEOS (*personal communication*)
- [19] US Weather Bureau, 1964, "Picture of the Month", *Monthly Weather Review*, vol.92 pp.76

- [20] “Soyuz Sovetskikh Sotsialisticheskikh Respublik: uchebnaya karta”, *Glavnoe Upravlenie Geodezii i Kartografii* (Moskva, 1969) - “Soviet Union: study map”, *Administration of Geodesy and Cartography* (Moscow, 1969), title translated by Dr Yelena Kalyuzhnova
- [21] Caspian Sea Facts, http://www.caspinfo.net/caspian_seafacts/climate/content.htm (*Last viewed on 20/07/2004*)
- [22] <http://www.cdc.noaa.gov/cdc/data.ncep.reanalysis.html> (*last viewed on 15/08/2005*)
- [23] <http://www.crh.noaa.gov/lot/webpage/beaufort/> (*last viewed on 15/08/2005*)
- [24] http://disc.gsfc.nasa.gov/data/datapool/AIRS/02.L2_Products/01_AIRX2RET/index.html (*Last viewed 16/08/2005*)
- [25] <http://www.eumetsat.int/en/>, *Historical Image Data Archive* (*last viewed on 18/08/2005*)
- [26] <http://www.savecaspiasea.com>, (*last viewed on 16/08/2005*)
- [27] <http://weather.uwyo.edu/upperair/soundings.html> (*last viewed on 16/08/2005*)
- [28] <http://www.wetterzentrale.de/topkarten/fsavneur.html> (*last viewed on 15/08/2005*)